Molecular Therapy
Nucleic Acids
Original Article

Non-invasive detection of allele-specific CRISPR-SaCas9-KKH disruption of *TOR1A* DYT1 allele in a xenograft mouse model

Katia E. Maalouf,[1,2,11] Dawn Madison Frederick,[1,11] Nutan Sharma,[2] Edwina Abou Haidar,[1] Tianhe Xiao,[1] Justin Seungkyu Han,[2] Mohammed S. Mahamdeh,[3,4,5] Roy J. Soberman,[5,6] David Rufino-Ramos,[7,8,9] Benjamin P. Kleinstiver,[7,8,9] Hyder A. Jinnah,[10] Christine A. Vaine,[2] D. Cristopher Bragg,[2] and Koen Breyne[1,2]

[1]Molecular Neurogenetics Unit, Department of Neurology, Massachusetts General Hospital and Harvard Medical School, Charlestown, MA 02129, USA; [2]The Collaborative Center for X-linked Dystonia-Parkinsonism, Massachusetts General Hospital, Charlestown, MA 02129, USA; [3]Division of Cardiology, Harvard Medical School, Boston, MA, USA; [4]Department of Medicine, Massachusetts General Hospital, Charlestown, MA 02129, USA; [5]Mass General Brigham Center of Excellence for Molecular Imaging, Charlestown, MA 02129, USA; [6]Division of Nephrology and Department of Medicine, Massachusetts General Hospital and Harvard Medical School, Charlestown, MA 02129, USA; [7]Center for Genomic Medicine, Massachusetts General Hospital, Boston, MA 02114, USA; [8]Department of Pathology, Massachusetts General Hospital, Boston, MA 02114, USA; [9]Department of Pathology, Harvard Medical School, Boston, MA 02115, USA; [10]Departments of Neurology and Human Genetics, Emory University School of Medicine, Atlanta, GA 30322, USA

DYT1 dystonia is a neurological movement disorder characterized by a dominant 3-base pair deletion (ΔGAG) in the *TOR1A* gene. This study demonstrates a gene-editing approach that selectively targets the ΔGAG mutation in the *TOR1A* DYT1 allele while safeguarding the wild-type (WT) *TOR1A* allele. We optimized an adeno-associated virus (AAV) vector-compatible variant of the *Staphylococcus aureus* Cas9 nuclease ortholog (SaCas9-KKH) in DYT1 patient-derived human neuronal progenitor cells (hNPCs). On-target editing of the *TOR1A* DYT1 allele was confirmed at the genomic level from brain tissue in a xenograft mouse model. To avoid brain biopsy for demonstrating *TOR1A* DYT1 editing, we developed a non-invasive monitoring method using extracellular RNA (exRNA). *TOR1A* exRNA was retrieved from the extracellular vesicle (EV) secretions of hNPCs and plasma samples, indicating whether the donor was a *TOR1A* DYT1 carrier. This technique enabled us to assess AAV-mediated disruption of the *TOR1A* DYT1 allele in the brains of mice using blood samples.

INTRODUCTION

DYT1 dystonia is a neurological disorder that manifests in childhood or adolescence, characterized by involuntary muscle contractions leading to abnormal movements and postures, and remains a challenging condition to treat effectively.[1] To enhance patients' motor function and overall quality of life, ongoing efforts include the continuous optimization of surgical therapies such as deep brain stimulation (DBS)[2,3] and the exploration of small-molecule drugs like ritonavir.[4] However, suboptimal responses or secondary exacerbations following DBS treatment[5] persist, alongside difficulties in attaining therapeutic drug concentrations within the central nervous system (CNS),[6] impeding patients' full recovery or sustained comfort.

Instead of treatment options primarily focusing on symptom management, a potential therapeutic intervention could be found by targeting the common signature mutation in DYT1 dystonia patients.[7–10] DYT1 patients carry a 3-bp deletion (c.907_909ΔGAG) in one *TOR1A* allele, known as the *TOR1A* DYT1 allele. This ΔGAG mutation results in the loss of a glutamic acid residue in the torsinA protein, which has been implicated in the pathogenesis of dystonia.[11] Genome editing with CRISPR-Cas enzymes is a promising approach for precisely targeting and disabling the *TOR1A* DYT1 allele. This approach aims to mitigate the disorder by addressing the dominant-negative effect, where a single copy of the allele with the ΔGAG mutation can cause DYT1 dystonia symptoms by impacting the function of the wild-type (WT) torsinA protein encoded by the *TOR1A* allele without the ΔGAG.[12]

In this study, we aim to tackle the limitations inherent to symptomatic dystonia treatments with a genome-editing strategy using smaller Cas9 orthologs that can be delivered by one single AAV vector. Utilizing the AAV9-compatible Cas9 ortholog from *Staphylococcus aureus* (SaCas9-KKH) editor,[13] we disrupted the *TOR1A* DYT1 allele in a xenograft mouse model. The preclinical DYT1 model was generated by implanting patient-derived human neural progenitor cells (hNPCs) in mouse brains,[14,15] allowing for the examination of human genetics and brain transduction after AAV treatment. DYT1 is a chronic disease, and gene editing is typically undertaken preemptively

Received 5 August 2024; accepted 24 January 2025;
https://doi.org/10.1016/j.omtn.2025.102466.

[11]These authors contributed equally

Correspondence: Koen Breyne, Ph.D., Molecular Neurogenetics Unit, Massachusetts General Hospital-East, 13th Street, Building 149, Charlestown, MA 02129, USA.
E-mail: kbreyne@mgh.harvard.edu

before symptom onset or during the early stages of mild symptoms. To maximize our AAV treatment's potential translational applicability, we anticipate that patients may seek confirmation of successful therapeutic intervention before observing improvements in symptoms. However, while detecting gene-editing activity at the genomic level is straightforward, genome analysis necessitates cell lysis, which poses challenges for brain tissue. A potential solution to this issue could involve analyzing the secretions from gene-edited brain tissue that enter the periphery, which can be analyzed following blood collection. Several studies have explored extracellular vesicles (EVs) released from the brain into the bloodstream, as they carry biomarkers for brain diseases.[16,17] Here, we demonstrate that extracellular RNA (exRNA) contained in EVs carries gene-editing information, and we show that these EVs can be used to assess brain cell editing through their leakage into the blood. Plasma collected from intracranially treated hNPC-implanted mice was used to evaluate the effectiveness of the AAV-Cas9-based editing approach on the *TOR1A* DYT1 allele and to monitor the status of the *TOR1A* allele lacking ΔGAG, without the need for invasive brain biopsy.

In conclusion, our study proposes gene editing to treat a hereditary neurological disease and leverages EVs as non-invasive biomarkers to predict therapeutic outcomes.

RESULTS

SaCas9-KKH-induced disruption of the *TOR1A* DYT1 allele in patient-derived neural progenitor cells

In the previous gene-editing study by Cruz et al., the strategy to target the *TOR1A* DYT1 allele involved using the engineered Cas9 variant from *Streptococcus pyogenes* (SpCas9-VRQR), which has shown incompatibility with single AAV-mediated gene therapy.[12] Here, we explored whether SaCas9-KKH, suitable for AAV-based genome editing, could target the *TOR1A* DYT1 allele. Four guide RNA (gRNA1–4) spacer sequences targeting the *TOR1A* DYT1 allele were designed (Figure 1A). Each spacer sequence contains a 5′ G to facilitate transcription initiated from the U6 promotor and targets a 20–23 sequence adjacent to the TGAGAT protospacer-adjacent motif (PAM) of SaCas9-KKH exclusively observed in the *TOR1A* DYT1 allele and not in the *TOR1A* WT allele without the ΔGAG. To screen gRNA1–4's efficiency of gene editing the *TOR1A* DYT1 allele with SaCas9-KKH, we incorporated them into sgRNA-expression plasmids with a U6 promoter and electroporated them, along with a SaCas9-KKH-2A-EGFP plasmid driven by a cytomegalovirus (CMV) promoter, in DYT1 patient-derived hNPCs (Figure 1B). After 5 days of culturing, SaCas9-KKH-expressing hNPCs were sorted by flow cytometry based on viability ($DAPI^{NEG}$) and eGFP fluorescence ($EGFP^{POS}$). Fluorescence-activated cell sorting (FACS) resulted in 10.5% ± 3.59% (mean ± SD) of hNPCs expressing SaCas9-KKH (Figure 1C). The sorted hNPCs were cultured until confluent to extract genomic DNA (gDNA) and subsequently assess the status of the *TOR1A* DYT1 allele. The genomic region of interest around the cleavage site was amplified (Table 1), and editing using gRNAs 1–4 was compared via next-generation CRISPR sequencing (NGS) and CRISPResso2 analysis.[18] All four gRNAs induced a significant percentage of edited NGS reads (33.2% ± 9.6%, mean difference ±SD) in the *TOR1A* DYT1 allele compared to the control condition without SaCas9-KKH (Figure 1D). We also evaluated the NGS reads of the *TOR1A* WT allele post SaCas9-KKH treatment, which had 29.4% ± 11.4% (mean difference ±SD) fewer edits than the observed on-target *TOR1A* DYT1 allele edits (Figure S1A). SaCas9-KKH nuclease activity induced various edits around the cleavage site in the *TOR1A* DYT1 allele, including deletions, substitutions, and insertions (Figure S1B). Deletions and insertions predominantly caused a premature stop codon in the *TOR1A* DYT1 allele (Figures S1C and S1D). Among the gRNA designs tested, gRNA 3 achieved the highest percentage of premature stop codons, with 37.3% ± 2.8% compared to 27.8% ± 4.8% (mean ± SD) for gRNA 1, gRNA 2, and gRNA 4 (Figure 1E). We also assessed seven potential off-target sites, identified by the Cas-OFFinder tool, for our top candidate, gRNA 3. gDNA from cells with confirmed on-target editing on the *TOR1A* DYT1 allele induced by SaCas9-KKH and gRNA3 was analyzed using NGS. The NGS analysis detected minimal to no edits in the potential off-target sites (Figure S1E). In conclusion, gRNA3 with SaCas9-KKH resulted in the highest editing efficiency and induced the most premature stop codons when targeting the *TOR1A* DYT1 allele while safeguarding the *TOR1A* allele without ΔGAG in hNPCs.

Detecting DYT1 dystonia signature using a ΔGAG-specific-TaqMan probe assay

Rapid detection of *TOR1A* DYT1 allele is essential for diagnostic purposes and to evaluate the therapeutic efficiency following gene-editing intervention. The trinucleotide disparity (small difference between DYT1 and WT alleles between healthy and DYT1 dystonia individuals) and the heterogeneous nature (mixture of both DYT1 and WT alleles in DYT1 dystonia patients) complicates the detection of DYT1 dystonia by conventional PCR/RT-qPCR, necessitating genomic sequencing to determine the disease. We designed a ΔGAG-specific assay that distinguishes between *TOR1A* WT (with GAG) and *TOR1A* DYT1 (without GAG) alleles on gDNA and cDNA levels with VIC and FAM (Fluorescein amidite) fluorophore-labeled TaqMan probes, respectively (Figure 2A). Our assay was initially tested using two custom-synthesized synthetic DNA sequences: one encoding the sequence of DYT1 patients surrounding ΔGAG to mimic the *TOR1A* DYT1 allele (248 bp) and the other encoding the sequence of healthy individuals with GAG (251 bp), referred to by *TOR1A* WT sequence (Table 2). The two synthetic DNA sequences were distinguishable by the relative fluorescence levels (ΔRn) of each allele-specific TaqMan probe, with a ΔRn of 6.2 for the ΔGAG-FAM probe targeting the *TOR1A* DYT1 sequence and a ΔRn of 4.7 for the GAG-VIC probe targeting the *TOR1A* WT sequence (Figure S2A). In comparison, ΔRn for the ΔGAG-VIC probe for the *TOR1A* DYT1 sequence was 0.25, and ΔRn for the ΔGAG-FAM probe for the WT sequence was 0.14. These ΔRn values could be visualized in a 2D plot identifying homozygous *TOR1A* DYT1 and homozygous WT sequences. Next, we assessed gDNA and transcript derived from healthy controls and DYT1 patient-derived hNPCs. In healthy control hNPCs, the ΔRn levels of the ΔGAG-FAM probe (0.21 ± 0.04 for gDNA and 0.02 ± 0.34 for

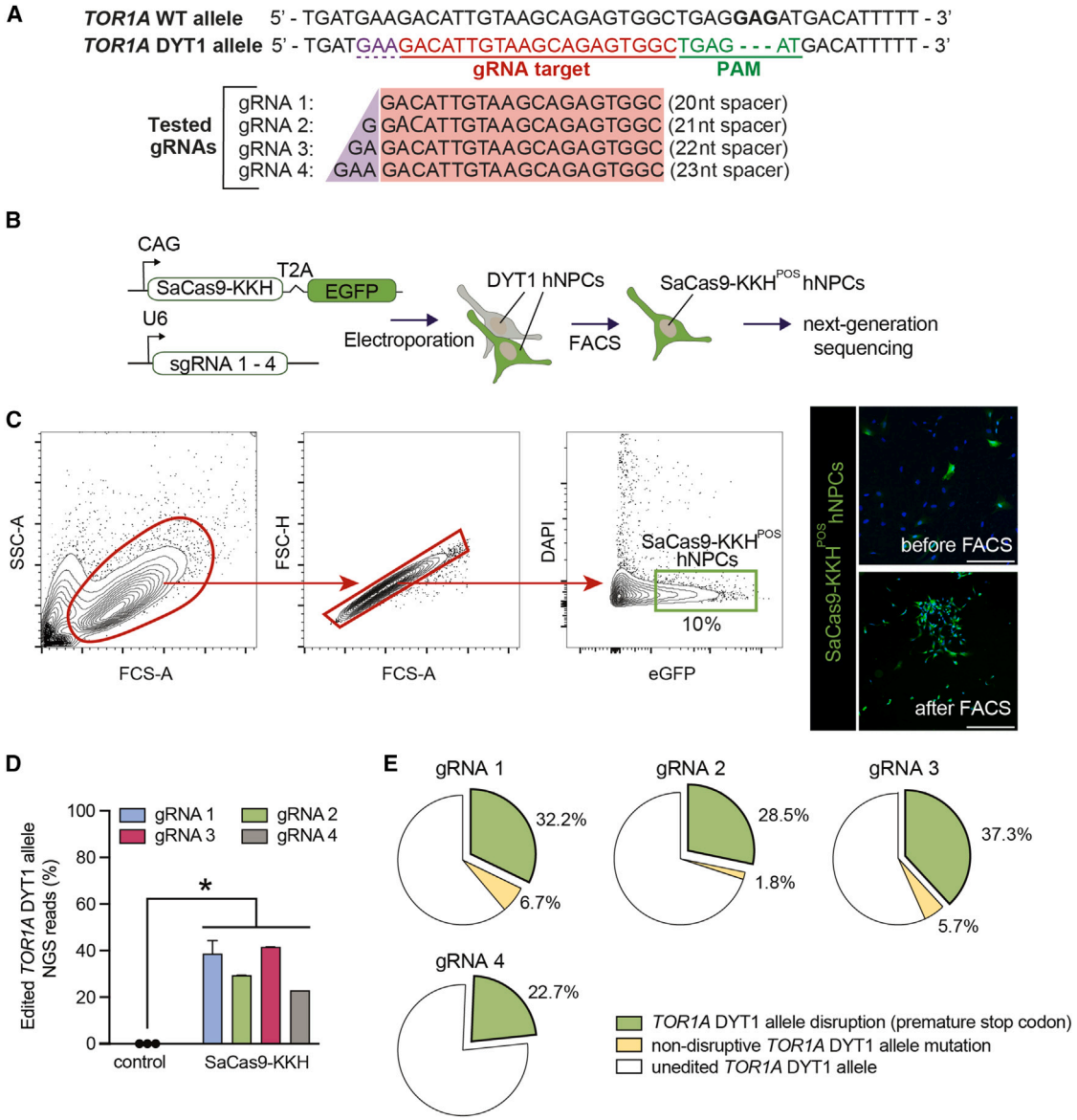

Figure 1. *TOR1A* DYT1 allele disruption by SaCas9-KKH nuclease activity in DYT1 hNPCs

(A) gRNA design to target the GAG deletion (ΔGAG) signature in DYT1 dystonia. The genomic sequence of the *TOR1A WT* and *TOR1A* DYT1 alleles in DYT1 dystonia patients. The 3-nucleotide (nt) difference between both alleles is indicated with a dotted line. The *TOR1A* DYT1 allele encodes a target site for gRNA1 to gRNA4 (highlighted in red) and a protospacer-adjacent motif (PAM; highlighted in green) for SaCas9-KKH. The gRNAs differ in length by the nucleotides upstream of the ΔGAG region, which are indicated in purple. (B) Screening of gRNAs in DYT1 hNPCs. This cartoon illustrates our screening process, where gRNA and SaCas9-KKH expression plasmids were electroporated into DYT1 hNPCs. Based on eGFP fluorescence encoded in the SaCas9-KKH plasmid, potentially gene-edited cells were isolated through FACS. The non-eGFP-expressing hNPCs were used as control. ΔGAG disruption was confirmed by analysis of next-generation sequencing. (C) Isolation of SaCas9-KKH-expressing DYT1 hNPCs. FACS gating strategy for selecting single live hNPC events ($DAPI^{NEG}$ $eGFP^{POS}$). Post electroporation, 9%–15% of the single live hNPC events are $eGFP^{POS}$. Images of SaCas9-KKH and eGFP-expressing hNPCs were taken using a confocal microscope. Scale bar represents 200 μM. (D) Gene editing of DYT1 allele in hNPCs with gRNA1–4 and SaCas9-KKH. Bar graph illustrating the percentage of editing of the *TOR1A* DYT1 allele based on next-generation sequencing analysis. gRNAs 1–4 targeted ΔGAG compared to hNPCs that did not express SaCas9-KKH (control). Statistical analysis was performed using a one-way ANOVA and GraphPad Prism 10.2.1 software. $^{*}p < 0.05$. (E) Types of genetic modifications introduced into the target DNA after gene editing of the *TOR1A* DYT1 allele in hNPCs. A pie chart generated by CRISPResso2 analysis illustrates the percentage of *TOR1A* DYT1 allele disruptions (i.e., premature stop codon), other mutations (i.e., insertions or deletions that did not result in a *TOR1A* DYT1 allele disruption or premature stop codon), and unedited alleles for gRNAs 1–4, with gRNA3 showing the highest level (37.3%) of premature stop codons.

Table 1. Primers and oligos used in Maalouf and Frederick et al.

Primers for preamplification of TOR1A cDNA and next-generation sequencing of cDNA	
cDNA_preamplification_DYT1_Forw	GCTCAAAGACATTGAACACGCG
cDNA_preamplification_DYT1_Rev	TCATCGTAGTAATAATCTAACTTGGTGAACACC
Dyt1 SaCas9-KKH gRNA oligos	
20nt top	caccGACATTGTAAGCAGAGTGGC
20nt bottom	aaacGCCACTCTGCTTACAATGTC
21nt top	caccGGACATTGTAAGCAGAGTGGC
21nt bottom	aaacGCCACTCTGCTTACAATGTCC
22nt top	caccGAGACATTGTAAGCAGAGTGGC
22nt bottom	aaacGCCACTCTGCTTACAATGTCTC
23nt top	caccGAAGACATTGTAAGCAGAGTGGC
23nt bottom	aaacGCCACTCTGCTTACAATGTCTTC
Dyt1 SaCas9 gRNA entry vector	
BPK2660	#70709
Primers used for next-generation sequencing of gDNA	
gDNA_preamp_forw	GTGGCTTCTGGCACAGCAG
gDNA_preamp_rev	TCAATCATCGTAGTAATAATCTAACTTGGTGAACAC
CRISPR_amp_fprw	CTCCCCCTGGAATACAAACACCT
CRISPR_amp_ rev	ATCATCGTAGTAATAATCTAACTTGGTGAACACC
Primers used for CRE-reporter cloning	
NLuc Forw	GGTTTTCCTTTGAAAAACACGATGATAATATGGCC ACACAATGGTCTTCACACTCGAAGATTTCGT
NLuc Rev	CGAGGCGCACCGTGGGCTTGTACTCGGTCATTGGGCCAGGATTCTCCTCGACGTC ACCGCATGTTAGCAGACTTCCTCTGCCCTCCGCCAGAATGCGTTC

transcript/cDNA, mean ± SD) were significantly lower than in our DYT1 hNPCs (2.16 ± 0.82 for gDNA and 2.83 ± 0.30 for transcript/cDNA, mean ± SD) ($p = 0.003$) (Figure S2B). The ΔRn levels of the GAG-VIC probe in the healthy control hNPCs (3.25 ± 0.29 for gDNA and 3.19 ± 0.32 for transcript/cDNA, mean ± SD) were higher than in our DYT1 sample (2.12 ± 0.07 for gDNA/2.23 ± 0.16 for transcript, mean ± SD). A 2D graph of the ΔRn levels of the TaqMan probes from both gDNA and transcript isolations showed that healthy control hNPCs clustered in the same region as the synthetic DNA encoding the *TOR1A* WT sequence (Figure 2B). Conversely, the ΔRn levels of DYT1 hNPCs clustered between those of the synthetic DNA encoding the ΔGAG mutation and the synthetic DNA encoding the *TOR1A* WT sequence. This was expected since the DYT1 hNPCs used in our analysis contained a single ΔGAG allele. Our findings with the ΔGAG-specific-TaqMan probe assay and hNPCs were confirmed in control and DYT1 patient-derived fibroblasts (Figure S2C). In conclusion, our ΔGAG-specific assay effectively distinguishes between healthy controls and DYT1 dystonia patients at both the genomic and transcriptional levels.

EVs secreted by cells derived from DYT1 dystonia patients carry the ΔGAG signature

Cells spontaneously release exRNA in the extracellular milieu.[19] We investigated whether hNPCs release *TOR1A* exRNA at detectable levels (Figure 3A). exRNA was extracted from conditioned medium derived from *TOR1A* DYT1 and healthy control hNPCs. Subsequently, cDNA was synthesized and preamplified using ΔGAG-flanking primers (Table 1) to prepare for ΔGAG or GAG (for *TOR1A* DYT1 and *TOR1A* WT sequences, respectively) assessment with the ΔGAG-specific TaqMan probe assay. Without this preamplification step, *TOR1A* exRNA derived from hNPC-conditioned medium could not be detected (Figure S3A). Additionally, the preamplification step helped exclude unwanted gDNA contamination by binding to exon 4 and exon 5 with the forward and reverse primers, respectively (Figure S3B), which we confirmed using an agarose gel and gDNA and cDNA derived from hNPCs (Figure S3C). exRNA can be found in the extracellular milieu through interaction with ribonucleoproteins (RNPs) or encapsulation into EVs.[20,21] To identify the carrier for *TOR1A* exRNA, we separated hNPC-EVs from RNPs through size-exclusion chromatography (SEC), which resolves particles in conditioned cell medium based on their size as they pass through a column of porous resin particles.[22] Preamplification of cDNA synthesized from *TOR1A* exRNA extracted from DYT1 and healthy control hNPC medium samples detected the expected 297-bp amplicon in pooled SEC fractions representing EVs (F6–F11), but not in those representing RNPs (F15–F20) (Figure 3B). Our next step was to validate whether *TOR1A* exRNA present in EVs could provide sufficient resolution to differentiate *TOR1A* DYT1 carriers from healthy control

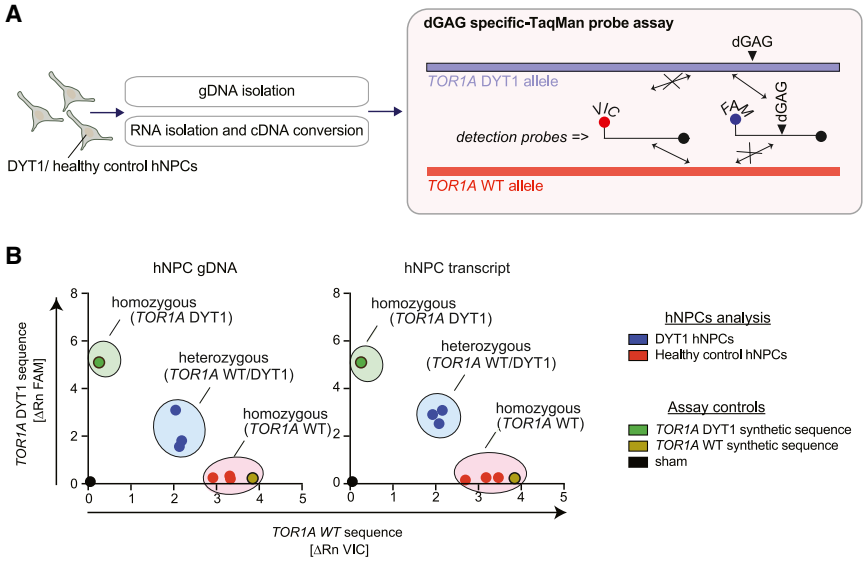

Figure 2. TaqMan probe assay for rapid detection of the ΔGAG signature in DYT1 dystonia

(A) ΔGAG-specific-TaqMan probe assay. Outline of genomic and transcript analysis of DYT1 and WT samples using GAG- or ΔGAG-targeting TaqMan probes labeled with either VIC or ΔGAG-FAM fluorophores, respectively. (B) hNPC analysis using a ΔGAG-specific TaqMan probe assay. The assay was evaluated with both gDNA (right) and cDNA (left) extracted from three DYT1 hNPCs (blue) and three WT control hNPCs (red). To validate the assay, gBlocks encoding exon 5 of the *TOR1A* allele with (green) and without (yellow) the ΔGAG mutation were used. A no-sample control was included (black dot).

individuals (Figure 3C). The ΔGAG-specific TaqMan probe assay was conducted on the *TOR1A* exRNA pre-amplicon, showing a cluster pattern similar to the transcript analysis of our hNPCs, distinguishing DYT1 from healthy control samples. Synthetic DNA assay controls containing *TOR1A* DYT1 or *TOR1A* WT sequences were included in our assessment of the *TOR1A* exRNA pre-amplicon. Considering the enhanced resilience and stability of exRNA within EVs in contrast to freely circulating exRNA,[20] we postulated that *TOR1A* exRNA containing ΔGAG sequences could be identifiable in EVs derived from the blood of DYT1 dystonia patients. exRNA was isolated from the plasma of *TOR1A* DYT1 carriers with or without manifesting symptoms and healthy controls (Figure 3D). The ΔGAG-specific TaqMan probe assay on the plasma samples confirmed that the *TOR1A* exRNA pre-amplicon was present in the blood and could identify *TOR1A* DYT1 carriers. The clustering in the 2D graph was irrespective of symptom occurrence in the *TOR1A* DYT1 carriers. In conclusion, we established that ΔGAG information present in *TOR1A* DYT1 carriers can be evaluated by analyzing cellular secretions or blood samples. This finding holds relevance for diagnostic applications without requiring an invasive biopsy.

TOR1A exRNA as a reporter for *TOR1A* DYT1 allele disruption in gene-edited hNPCs

Disruption of the *TOR1A* DYT1 allele by SaCas9-KKH activity induces non-homologous end-joining (NHEJ) repair, resulting in genetic changes around the targeted cleavage position.[23] If an easily screenable phenotype is not observed following SaCas9-KKH activity, as encountered with DYT1 dystonia versus healthy controls in hNPC cultures, a comprehensive genotype analysis involving cell lysis, gDNA extraction, and NGS is required. We hypothesized, based on our ΔGAG-specific TaqMan probe assay observations, that assessing *TOR1A* exRNA in the secretions of hNPCs would provide a non-damaging alternative to genomic assessment of cells to evaluate disruptions following SaCas9-KKH targeting of the *TOR1A* DYT1 allele.

The primary requirement is that the *TOR1A*-derived transcript, the source of exRNA in DYT1 hNPCs, accurately reflects the *TOR1A* DYT1 status in the gDNA. Analysis of both gDNA and RNA/cDNA from DYT1 hNPCs exhibited an expected 50:50 DYT1:WT allele ratio when considering the 17-bp region upstream of the ΔGAG site in the *TOR1A* gene (Figure 4A). NGS analysis of both gDNA and RNA/cDNA confirmed that the same region in healthy control hNPCs does not carry the *TOR1A* DYT1 mutation (Figure S3D). Next, we isolated exRNA from DYT1 hNPCs and verified whether the *TOR1A* DYT1 information could also be detected with NGS (Figure 4B). We also confirmed that EV transcripts contain the 50:50 DYT1:WT *TOR1A* allele when considering the 17-bp region upstream of the ΔGAG site in the *TOR1A* gene. To assess whether *TOR1A* exRNA is a reliable readout for the disruption of the *TOR1A* DYT1 allele, DYT1 hNPCs were electroporated with SaCas9-KKH^{POS}- and sgRNA3^{POS}-encoding plasmids prior to FACS and culturing of *TOR1A* DYT1-targeted hNPCs for EV secretion. Analysis of exRNA from SaCas9-KKH- and sgRNA3-expressing hNPCs showed a decrease in NGS reads of the *TOR1A* DYT1 allele and the occurrence of insertions and deletions around the targeted cleavage site (Figure 4C). However, exRNA tends to underreport *TOR1A* DYT1 disruption. While 41.5% of the *TOR1A* DYT1 allele shows changes at the gDNA level in DYT1 hNPCs, exRNA indicates that only 9.4% of the *TOR1A* DYT1 allele is disrupted (Figure 4D). To evaluate the capability of exRNA in reporting *TOR1A* DYT1 editing in their hNPC-donor cells, we analyzed EVs and their donor hNPCs after gene editing with the top three performing gRNAs (gRNAs 1, 2, and 3) using our *TOR1A* DYT1-specific TaqMan probe assay (Figure 4E). To compare edited and non-edited EVs/hNPCs, we performed FACS separation of SaCas9-KKH/GFP^{POS} and SaCas9-KKH/GFP^{NEG} hNPCs prior to EV secretion, exRNA isolation, and EV-donor hNPC transcript isolation. We conducted a correlation analysis in parallel on both the transcript of the hNPCs and their exRNA with our ΔGAG-specific TaqMan probe assay. Our negative control (SaCas9-KKH/GFP^{NEG}), expected to lack edits in the *TOR1A* DYT1 region (Figure S3E), exhibited high Rn levels of the ΔGAG-FAM TaqMan probe in both our DYT1 hNPCs and their exRNA (gray circle in Figure 4F). However, the Rn levels of the

Table 2. DYT1 and WT synthetic DNA sequences used in Maalouf and Frederick et al.

TOR1A WT sequence	GTGGCTTCTGGCACAGCAGCTTAA TTGACCGGAACCTCATTGATTATT TTGTTCCCTTCCTCCCCCTGGAAT ACAAACACCTAAAAATGTGTATCC GAGTGGAAATGCAGTCCCGAGGC TATGAAATTGATGAAGACATTGTA AGCAGAGTGGCT**GAGGAG**ATGAC ATTTTTCCCCAAAGAGGAGAGAG TTTTCTCAGATAAAGGCTGCAAA ACGGTGTTCACCAAGTTAGATTA TTACTACGATGATTGA
TOR1A DYT1 sequence	GTGGCTTCTGGCACAGCAGCTT AATTGACCGGAACCTCATTGAT TATTTTGTTCCCTTCCTCCCCCTGG AATACAAACACCTAAAAATGTGTA TCCGAGTGGAAATGCAGTCCCGAG GCTATGAAATTGATGAAGACATTG TAAGCAGAGTGGCTGAGATGACA TTTTTCCCCAAAGAGGAGAGAGTT TTCTCAGATAAAGGCTGCAAAACG GTGTTCACCAAGTTAGATTATTACT ACGATGATTGA

ΔGAG-FAM probe in SaCas9-KKH-expressing hNPCs dropped significantly for all three gRNAs due to *TOR1A* DYT1 editing (p = 0.0002) (green circle in Figure 4F). The reduction in the intact *TOR1A* DYT1 due to SaCas9-KKH activity compared to non-edited hNPCs was 23.02% ± 1.58% (Δ mean ± SED), and 34.76% ± 8.59% (Δ mean ± SED) in the exRNA derived from the hNPC cells. To enable this comparison using the ΔGAG-FAM probe, the data were normalized to the GAG-VIC probe. In conclusion, we demonstrated that exRNA carried by EVs serves as a reporting tool for monitoring edited events on the *TOR1A* DYT1 allele in their donor cells.

Targeting of mouse brain implanted hNPCs with AAV9

We chose AAV9 as the carrier for our gene-editing machinery due to its high efficiency in delivering genetic material to the CNS, making it ideal for targeting neurological diseases and brain disorders.[24,25] To evaluate the efficacy of AAV9 in targeting hNPCs, we utilized a CRE traffic light reporter system that was expressed in hNPCs by lentiviral transduction and puromycin selection (Figure 5A). CRE activity encoded by AAV9 is expected to interact with the reporter system, switching the fluorescence from red (off state) to green (on state) (Figure 5B). hNPCs were transduced with the AAV9-CMV enhancer/chicken β-actin (CBA)-CRE vector, and green fluorescence (on state) was observed, indicating functional CRE delivery and reporter activation (Figure 5C). Green fluorescence was not observed in our phosphate-buffered saline (PBS)-exposed *in vitro* condition. To assess AAV9 activity *in vivo*, 200,000 of our CRE traffic light reporter-expressing hNPCs were implanted intracranially with AAV9-Cre in nude mice (Figure 5D). Twenty-one days post injection of ∼2 × 10^{10} genome copies (gc)/kg AAV9-CBA-CRE or AAV9-null and implantation of hNPCs, the xenografts in the mouse brains were analyzed for green fluorescence in coronal sections. hNPCs implants exposed to AAV9-CBA-CRE showed 67% ± 10% (Δ mean ± SED) more cells with green fluorescence (on state) than our AAV9-null condition (Figure 5E). Upon microscopic examination of the brains, the disparity in fluorescence between our experimental conditions was confirmed (Figure 5F). In conclusion, our findings demonstrate the effective transduction of implanted hNPCs by AAV9, highlighting its potential as a promising capsid for delivering CRISPR genome-editing tools in the brain.

Disruption of the *TOR1A* DYT1 allele *in vivo* with AAV9-SaCas9-KKH

To assess *TOR1A* DYT1 allele targeting in the brain using genome editing, gRNA 3 was cloned into an all-in-one AAV backbone with SaCas9-KKH[26] and packaged into an AAV9 capsid, referred to as AAV9-SaCas9-KKH (Figure 6A). DYT1 hNPCs implanted into the striatum of nude mice were intracranially treated with approximately 2 × 10^{10} gc/kg of either AAV9-SaCas9-KKH or AAV9-null (empty AAV9 capsid). After 21 days, the mice were sacrificed to collect cardiac blood and/or brain tissues. exRNA and gDNA were isolated from each sample respectively and used in downstream NGS analysis. Three *in vivo* experiments were conducted (Figure S4A). In experiments 1 and 3, we analyzed the hNPC implant treated with AAV9-SaCas9-KKH or AAV9-null. gDNA was isolated from coronal brain sections containing our treated hNPCs, and PCR amplicon surrounding the ΔGAG region was generated to be compatible with NGS and CRISPResso2 analysis.[19] Sequence analysis revealed edits in the DYT1 allele at the target site in the AAV9-SaCas9-KKH-treated samples, whereas no such edits were observed in the AAV9-null-treated brains (Figure S4B). We quantified the edits in both conditions and found significantly more *TOR1A* DYT1 allele editing in the AAV9-SaCas9-KKH samples compared to the AAV9-null samples (3.6% ± 1.64% vs. 0.7% ± 1.09%, mean ± SD, respectively) (Figure 6B). In experiments 2 and 3, we analyzed the plasma of the xenograft mice to determine whether exRNA could indicate whether our genome-editing therapeutic intervention in the brain successfully altered *TOR1A* DYT1 in the DYT1 hNPCs (Figure S4A). An amplicon was generated after isolating exRNA and cDNA conversion to be assessed with NGS and CRISPResso2 analysis. *TOR1A* DYT1 allele edits due to SaCas9-KKH activity could be observed in the AAV9-SaCas9-KKH conditions (Figure S4C). Notably, the NGS reads encoding the *TOR1A* DYT1 region derived from hNPC exRNA were rare and truncated, necessitating filtering to extract relevant information about the modified *TOR1A* DYT1 allele. These reads did not capture all the edit variations observed in the brain tissue samples. Nonetheless, edited *TOR1A* DYT1 allele reads were significantly more prevalent in the plasma of the AAV9-SaCas9-KKH treated group compared to the AAV9-null-treated group (Figure 6C). In conclusion, AAV9-SaCas9-KKH effectively targets the *TOR1A* DYT1 region in the brain of a xenograft DYT1 model, and the impact of the gene editing can be assessed through blood analysis.

DISCUSSION

Gene editing in the brain is promising for treating hereditary neurological diseases.[27] Previously, the potential of gene editing had been

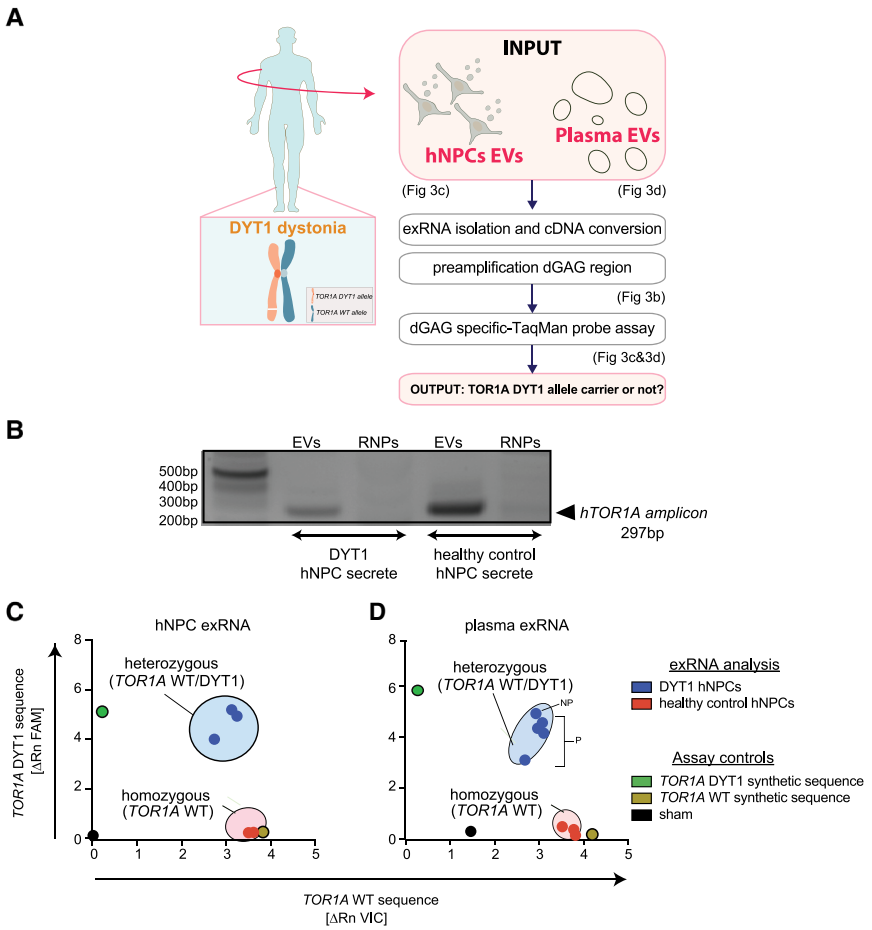

Figure 3. EVs carry the ΔGAG signature when secreted from DYT1 hNPCs and are present in DYT1 patient plasma

(A) Screening for ΔGAG in EVs derived from DYT1 patients. Cartoon illustrating our setup for isolating exRNA from hNPC-derived EVs in conditioned culture medium as well as EVs from patient plasma. Following exRNA isolation and cDNA conversion, we performed preamplification of the ΔGAG region, which was subsequently analyzed using a ΔGAG-specific TaqMan probe assay. (B) The ΔGAG region pre-amplicon is exclusively found in EV-derived exRNA. We evaluated the presence of the ΔGAG region in fractions containing EVs and ribonucleoproteins (RNPs) following SEC of conditioned hNPCs culture medium. Our data, represented by preamplification PCR results loaded on agarose gel, showed bands in the EV fractions for both WT and DYT1 samples, while no bands were observed in the RNP fractions. (C) ΔGAG-specific TaqMan probe assay as a screening tool to detect ΔGAG in EVs derived from DYT1 hNPCs. A 2D plot distinguishes exRNA from three DYT1 hNPCs (blue) and three WT control hNPCs (red). The assay involved performing preamplification PCR on cDNA-transformed exRNA to ensure the detection of the GAG-VIC and ΔGAG-FAM probes, specifically within hNPC-derived EVs. gBlocks controls with (green) and without (yellow) the ΔGAG mutation were used. A no-sample control was included (black dot). (D) ΔGAG in plasma from DYT1 patients. A 2D plot distinguishes exRNA from plasma samples collected from eight patients using a ΔGAG-specific TaqMan probe assay. The colors and controls correspond to those in (C). P and NP denote DYT1 patients presenting with or without symptoms, respectively.

explored for DYT1 dystonia, selectively targeting the *TOR1A* DYT1 allele while safeguarding the *TOR1A* WT allele in patient-derived fibroblasts.[12] However, due to its ∼4.1-kb size, the strategy using the engineered Cas9 variant from *S. pyogenes* (SpCas9-VRQR) proved incompatible with single AAV-mediated gene editing. Therefore, we developed an alternative Cas-based approach to facilitate the translation of these promising gene-editing techniques to clinical applications. A more compact SaCas9-KKH editor,[13] ∼3.2 kb in size, was utilized and tested on hNPCs, which more closely resembled the target cell type for DYT1 dystonia than fibroblasts. Despite the resilience of hNPCs to transfection, ∼30%–40% editing was achieved in the DYT1 allele with SaCas9-KKH and gRNA-encoding plasmids. Notably, ∼75%–90% of these edits resulted in the induction of a premature stop codon downstream of the mutation. However, when the gene-editing machinery was delivered by AAV to hNPCs when implanted in the brains of mice, the efficiency of gene editing was reduced 10-fold compared to our *in vitro* results. This discrepancy may be attributed to the mosaicism present *in vivo*. In contrast, this issue was mitigated *in vitro* using FACS to analyze only SaCas9-KKH^{POS} cells, ensuring a more uniform editing efficiency. Indeed, using the CRE-reporter system, it was determined that the AAV9 capsid successfully targeted the majority of hNPCs in the brain, with ∼20% of the implanted hNPCs not being transduced. Additionally, while the powerful CBA promoter successfully drove SaCas9-KKH expression *in vitro*, its size constraints prevented it from fitting within our AAV vector. Consequently, we switched to a CMV promoter, which can be methylated *in vivo*, resulting in reduced effectiveness. Our technology offers the potential to address the DYT1 dystonia-associated mutation in the brain; however, further improvements are needed to enhance its suitability for clinical applications. AAV9 vectors are highly effective for direct in-brain injections and are being evaluated for treating neurological disorders[28]; however, factors such as dose, age at the time of injection, and preexisting neutralizing antibodies in the host are critical determinants of their safety and efficacy.[29] As the gene therapy field advances, alternative strategies are emerging, including systemic injections with liver-detargeted AAV capsid variants[30,31] and non-viral carriers.[32] Likewise, for gene editing, hypercompact editors, novel editing strategies, or more efficient editors can be explored to enhance ΔGAG editing outcomes.[33]

DYT1 dystonia is a chronic condition characterized by progressive involuntary muscle contractions that lead to repetitive or twisting movements and abnormal postures.[10,34] Symptoms of DYT1 dystonia generally start to manifest during childhood, typically with an average

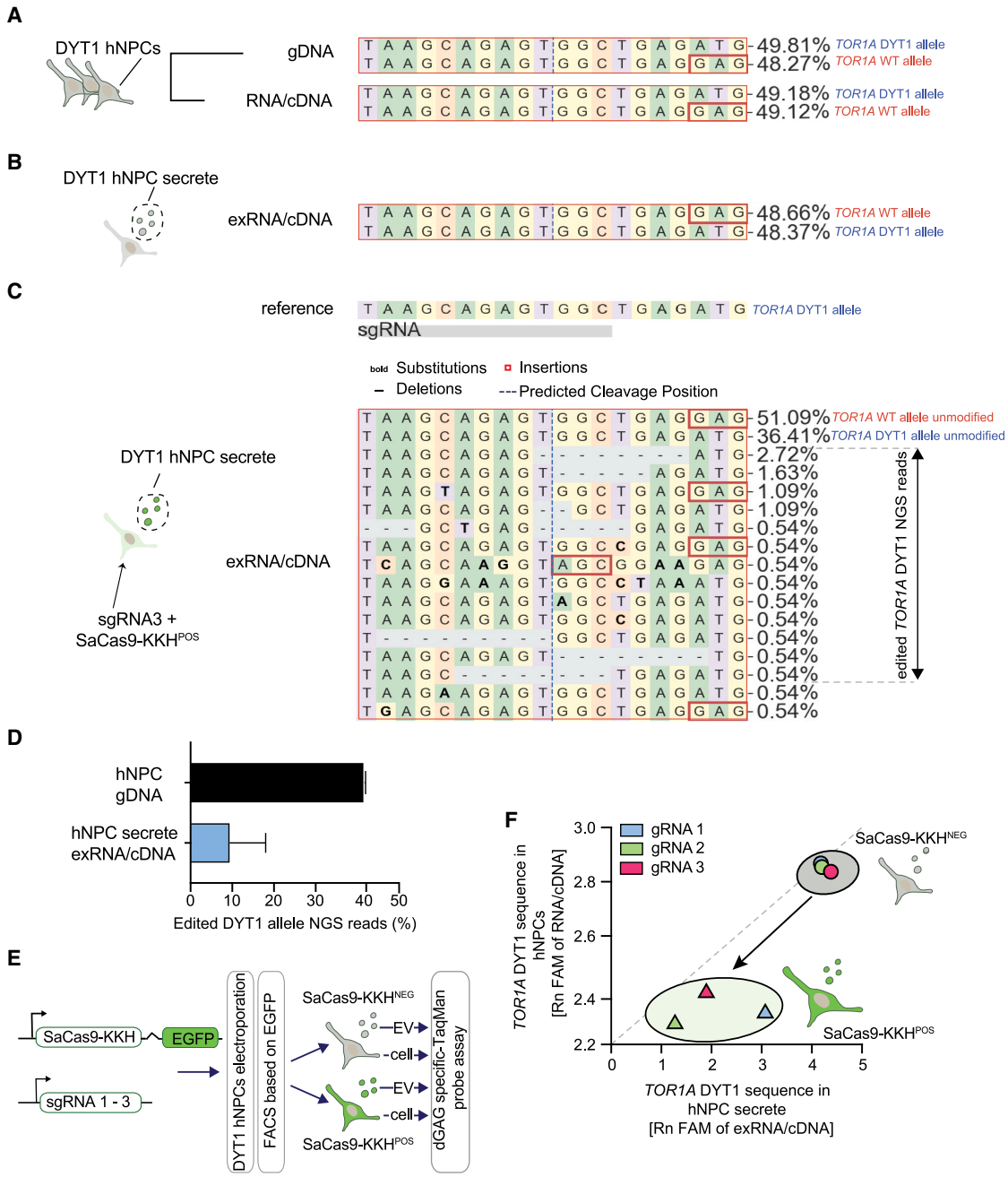

Figure 4. EVs as non-invasive biomarkers for mutant allele disruption by SaCas9-KKH nuclease activity in DYT1 hNPCs

(A) ΔGAG signature in DYT1 hNPCs. Next-generation sequencing analysis of gDNA and cDNA-converted transcript isolates. (B) ΔGAG signature in EVs derived from DYT1 hNPCs. Next-generation sequencing analysis of cDNA-converted exRNA. (C) exRNA as a biomarker for gene editing of the ΔGAG region in the DYT1 allele. Representative next-generation sequencing result revealing indels in exRNA-converted cDNA from DYT1 hNPCs expressing gRNA 3 and SaCas9-KKH. (D) Underreporting of DYT1 allele editing by EVs compared to donor cells. A comparison of indels from next-generation sequencing analysis of DYT1 hNPCs electroporated with SaCas9-KKH and gRNA 3 and their corresponding EVs. (E) Gene-editing reporting in EVs vs. cells. Schematic of data (F). DYT1 hNPCs were electroporated with SaCas9-KKH and gRNAs 1–3, followed by FACS of eGFP-positive ($DAPI^{NEG}$ $eGFP^{POS}$) and eGFP-negative ($DAPI^{NEG}$ $eGFP^{NEG}$) cells. These sorted hNPCs were cultured and analyzed using the ΔGAG-specific TaqMan probe assay as well as their exRNA in the conditioned medium. (F) Changes in ΔGAG levels in DYT1 hNPCs following CRISPR-Cas activity are mirrored in their EVs. A 2D plot displays ΔGAG-FAM levels in cDNA from cell transcripts and EV exRNA from edited and non-edited cells. These levels were normalized to the GAG-VIC probe to establish a correlation between hNPCs and their EVs. The drop along the dotted line in the cluster after gene editing indicates that DYT1 allele targeting can be detected in both EVs and cells. Label colors represent the different gRNAs used.

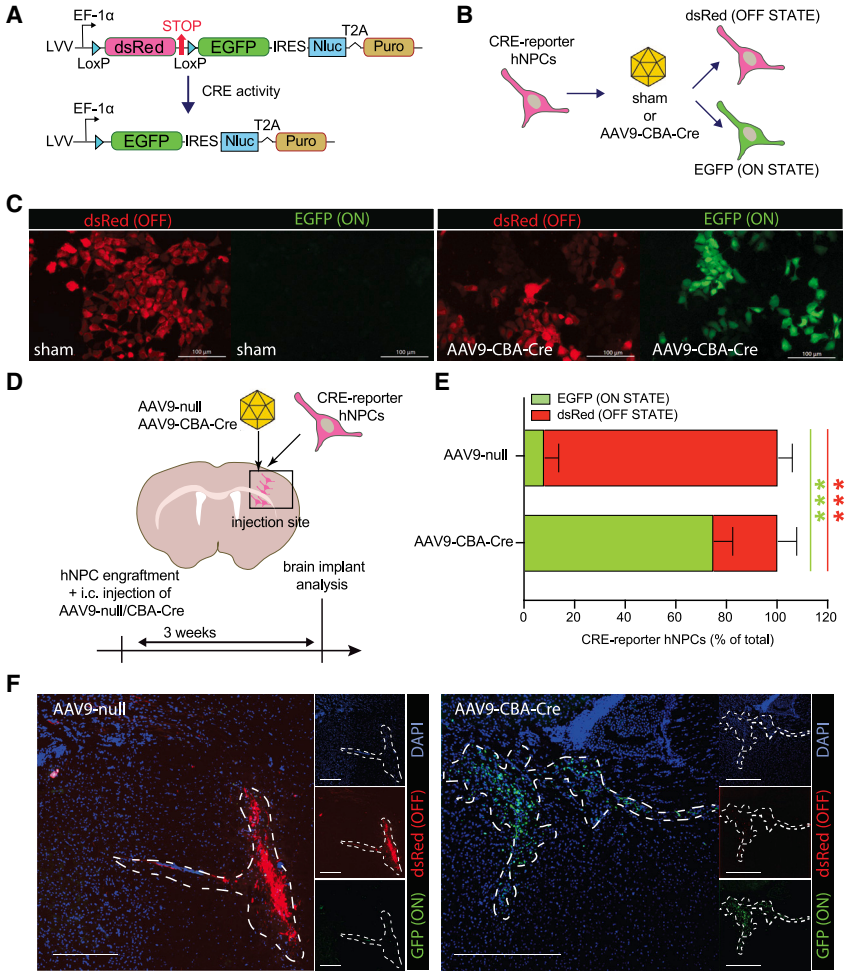

Figure 5. AAV-mediate transgene-delivery to hNPCs engrafted in a mouse brain

(A) CRE reporter to detect CRE activity. A schematic of a lentiviral vector (LVV) encoding a CRE reporter (Addgene #62732) is shown. The reporter includes a floxed dsRed cassette followed by eGFP, nanoluciferase (Nluc), and puromycin transgenes. CRE activity is monitored by blocking eGFP expression downstream of dsRed with a stop codon (OFF STATE). Upon CRE delivery, dsRed is excised, enabling eGFP expression (ON STATE). The expression of Nluc and puromycin remains unaffected by the floxing status due to the preceding IRES site. Nluc is used to select brain sections with implanted hNPCs, while puromycin is used to select hNPCs containing the reporter. (B) CRE-reporter hNPCs. A cartoon illustrating CRE reporting in hNPCs to track AAV transduction events. The reporter is introduced into hNPCs via LVV transduction followed by puromycin selection. Following AAV delivery, CRE activity causes the CRE-reporter hNPCs to transition from red to green fluorescence, visually indicating the successful excision of the reporter. (C) *In vitro* transduction of CRE-reporter hNPCs with AAV9-CBA-CRE. Three days post exposure of ~2 × 1010 gc AAVs to Cre-reporter-hNPCs, >60% of hNPCs exhibit eGFP expression, while nontransduced hNPCs maintain dsRed fluorescence. The scale bar represents 100 μm. (D) hNPC implantation mouse model. A cartoon illustrates the intracranial (i.c.) injection of CRE-reporter-hNPCs and AAV9-CBA-CRE in mice. The black square highlights the specific brain region with implanted hNPCs, as shown in (F) and quantified in (E). The timeline on the bottom shows the timeline of the experimental interventions. (E) CRE activity post AAV9-CBA-CRE administration in the hNPC-implantation mouse model. Red (OFF STATE) and green (ON STATE) fluorescent hNPCs were quantified in brain sections. Statistical analysis was conducted using Student's t test; ***$p < 0.001$. (F) AAV transduction of hNPCs in the mouse brain. The left panel shows the expression pattern of CRE-reporter-hNPCs with AAV9-null (empty vector) administration, where dsRed fluorescence is observed. Following an i.c. injection of approximately 2 × 10^{10} gc/kg AAVs, green fluorescence in the right panel indicates AAV9-CBA-CRE transduction of hNPCs after brain implantation. This is a representative image, with multiple samples analyzed and quantified in (). Scale bar represents 100 μm.

of 12 years.[35] Gene-editing therapies present an opportunity for early intervention, potentially achieving comprehensive editing of target cells before disease progression complicates treatment strategies. Genome-editing therapies for DYT1 dystonia could thus be envisioned as an approach to positively impact physiological processes affected by the *TOR1A* DYT1 mutation. Assessing successful gene editing in the brain is challenging, particularly without resorting to brain biopsy. Therefore, we tested whether EVs could be used in the context of dystonia to identify new biomarkers for DYT.[36] EVs are small membrane-bound structures released by cells into the extracellular milieu and that play a pivotal role in intercellular communication and are increasingly recognized as valuable indicators of neurological disease progression.[37] They encapsulate various molecules, including proteins and exRNA, reflecting the cellular state and genetic alterations.[38] The use of EVs has emerged as a promising vehicle for delivering gene-editing components.[39–44] However, leveraging EVs to monitor gene-editing outcomes represents a novel paradigm in the field, granting the ability to monitor changes in the nucleus without having to lyse the cell. Here, we first tested whether cell transcripts, which are essential for exRNA assessment, accurately reflect edits in the *TOR1A* DYT1 allele at the genomic level, and we validated this using a ΔGAG-specific TaqMan probe assay and NGS. We then analyzed the exRNA from cultured DYT1 hNPCs and isolated it from plasma, confirming the presence of the *TOR1A* DYT1 allele. Finally, we investigated the presence of EVs released from hNPCs implanted in the brain into the periphery, aiming to monitor the levels of *in vivo* SaCas9-KKH genome editing in hNPCs into a larger number of mouse brain cells. Our findings indicated edits in the *TOR1A* DYT1 region, along with the detection of truncated exRNA-derived fragments.

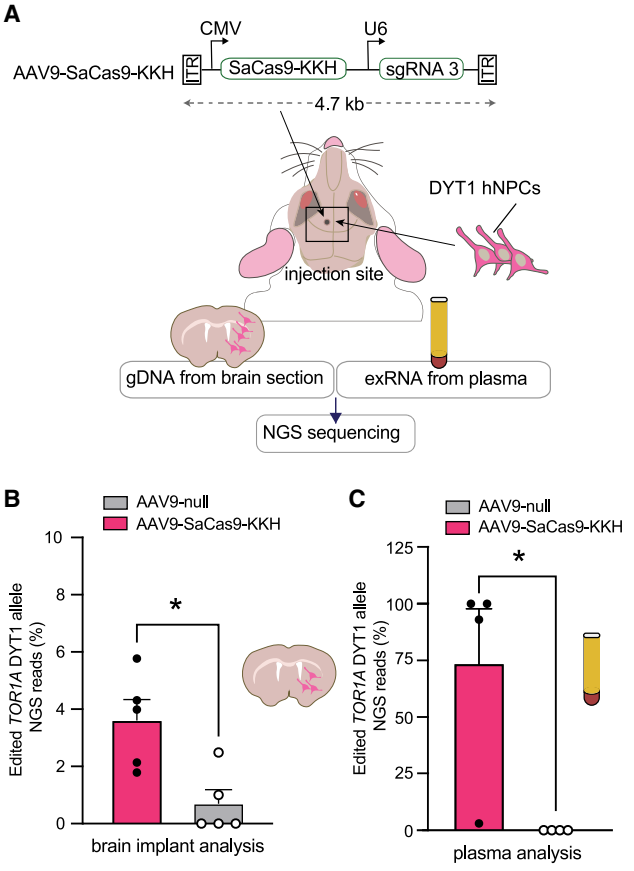

Figure 6. *In vivo* targeting of ΔGAG with AAV9-CRISPR

(A) hNPC-implantation mouse model to test gene therapy for treating ΔGAG in the brain. A schematic illustrates the i.c. injection of DYT1 hNPCs treated with either AAV9-CRISPR or AAV9-null. After 21 days, cardiac blood and brain tissues were collected, followed by the isolation of exRNA from the plasma and gDNA from brain sections with hNPCs, and subsequent next-generation sequencing analysis. The AAV9-CRISPR construct is illustrated at the top. (B) Detection of ΔGAG edits in the brain. CRISPResso2 analysis reveals a higher percentage of DYT1 allele edits in injected hNPCs from AAV9-CRISPR samples (pink) compared to AAV9-null samples (gray). Statistical analysis was conducted using Student's t test; $^*p < 0.05$. (C) Detection of ΔGAG edits in plasma. CRISPResso2 analysis of exRNA-converted cDNA isolated from the plasma of injected mice shows edits in the mutant allele of the released *TOR1A* transcript in AAV9-CRISPR samples (pink), but not in AAV9-null samples (gray). Statistical analysis was conducted using Student's t test; $^*p < 0.05$.

In summary, this study introduces a non-invasive framework proposing EVs as potential biomarkers for monitoring *TOR1A* DYT1 disruption in the brain, which is implicated as the underlying cause of DYT1 dystonia symptoms targeted by AAV-mediated gene-editing intervention.

MATERIALS AND METHODS

Cell culture

Coded patient-derived fibroblasts from DYT1 patients (33115, 33217, 34866) and healthy controls (33114, 33362, 33113) were grown in culture plates with Dulbecco's modified Eagle's medium (DMEM/Nutrient Mixture F-12 (F12) (Thermo Fisher Scientific, Waltham, MA, USA) supplemented with 20% fetal bovine serum (FBS) (GeminiBio #900-108, West Sacramento, CA, USA). Coded induced pluripotent stem cell (iPSC)-derived hNPCs were generated from DYT1 patient fibroblasts (DYT1-1, 2551B, 30857C) and healthy controls (AK3, 33362C, 331132i) as previously described for X-linked dystonia-parkinsonism hNPCs.[45,46] NPCs were grown on Geltrex-coated (Thermo Fisher Scientific, #A1413302) tissue culture ware in DMEM/F12 (Thermo Fisher Scientific) supplemented with 2% B27 (Gibco, #17504044, Grand Island, NY, USA), 20 ng/mL epidermal growth factor (EGF) (PeproTech # AF-100-15, Cranbury, NJ, USA), 20 ng/mL fibroblast growth factor (FGF) (Millipore Sigma, Burlington, MA, USA), 0.2% heparin (STEMCELL Technologies #07980, Cambridge, MA), and 1% penicillin-streptomycin (Corning #30-002-C, Manassas, VA, USA). HEK293T cells from M. Calos (Stanford University, Stanford, CA) were cultured using DMEM supplied with 10% FBS (Sigma-Aldrich, St. Louis, MO, USA) and 1% penicillin-streptomycin (Corning #30-002-C). Cells were routinely tested for mycoplasma contamination (Mycoplasma PCR Detection Kit, abm G238, Richmond, Canada) and found negative.

Participant recruitment and sample collection

Plasma samples and phenotype data were obtained from the Dystonia Partners Research Bank, which is a tissue and databank approved by the Mass General Brigham Institutional Review Board (protocol # 2011P000110). All participants provided written informed consent for their samples and data to be used for genetic and cellular analyses. Whole blood was collected into 10-mL EDTA tubes. Within 2 h of collection, tubes were centrifuged at 1,100 × *g* at room temperature (RT) for 10 min to separate the plasma from cells. Plasma was removed from the upper layer using a pipette, then filtered through 0.8-μm Millipore filters, and aliquoted into Cryovials in volumes of 0.5–1 mL and stored at −80°C.

Phenotypic Data

Samples 33115, 33217, 34866, 42375, and 40890 were collected from individuals affected with DYT1 dystonia. Four participants were male (33115, 33217, 42375, and 40890) and one was female (34866). For every affected participant, onset began in childhood and diagnosis was confirmed by clinical genetic testing. Samples were collected at the following ages: 33115 collected at 19 years old, 33217 collected at 22 years old, 34866 collected at 62 years old, 42375 collected at 22 years old, and 40890 at 13 years old. Sample 42374 was collected from a non-manifesting, female carrier of the DYT1 mutation who was examined and provided a sample at the age of 30 years.

Samples 33113, 33114, 33362, 37043, 39910, and 42376 were collected from neurologically normal individuals. Two participants were male (33114 and 33362) and four participants were female (33113, 42376, 37043, and 39910). Samples were collected, and the participants examined, at the following ages: 55 years old (33113), 46 years old (33114), 29 years old (33362), 62 years old (42376), 26 years old (37043), and 47 years old (39910).

gRNA cloning

gRNA entry vector plasmid BPK2660 (Addgene plasmid #70709) was digested using the enzyme BsmSMBI-v2 (New England Biolabs #R0580, Ipswich, MA, USA). Oligos were annealed using T4 DNA ligase buffer (New England Biolabs #M0202S) at a temperature of 95°C for 5 min and cooled to 10°C at a ramp rate of -5°C/min. The digested vector backbone and annealed gRNA oligo were ligated using T4 DNA ligase (New England Biolabs #M0202S), transformed into NEB Stable Competent *E. coli* (New England Biolabs #C3040H), and plated on Luria Broth plates with ampicillin. Colonies were screened with a high-fidelity amplification (forward: TTTCCCCGAA AAGTGCCACCTGGTCGACATTGATTATTGATGTACAAAAAA GCAGGCT. Reverse: GCTATGAACTAATGACCCCGTAATTCAT TACTATTAATAAAAAAAAAAATCTCGCCAACAAGTTGACG) followed by a digest of the PCR product using BSMB1-v2 (New England Biolabs #R0580). Rapid plasmid sequencing was conducted on the plasmid to ensure correct sequence.

Nucleofection of plasmids encoding gRNAs and SaCas9-KKH

P4 Primary Cell 4D-Nucleofector X Kit L (LONZA, #V4XP-4024, Cologne, Germany) was used for the nucleofection of hNPCs. Falcon six-well tissue culture plates (Life Sciences #353046, Corning, NY, USA) were coated with Geltrex (Thermo Fisher Scientific #A1413302). A 50-mL aliquot of cell culture medium was prewarmed. 800,000 cells were resuspended in 100 μL of RT 4D Nucleofector solution (80 μL of Nucleofector solution and 20 μL of Nucleofector supplement). 2 μg of SaCas9-KKH plasmid and 2 μg of gRNA were added to the resuspended cells. The resuspension was transferred to a 100-μL single Nucleocuvette. Cells were nucleofected using a 4D-Nucleofector core unit. After nucleofection, 500 μL of prewarmed cell culture medium was immediately added and the cells were plated in a precoated six-well plate with 3 mL of cell culture medium. Cells were then spun at 70 × *g* for 3 min to ensure proper attachment. Medium was changed after 72 h. Five days post nucleofection, the cells went through FACS where GFP-positive and GFP-negative cells were sorted. Both conditions were plated in a 48-well plate and cultured until confluent.

FACS

Cells were detached using Accutase (Corning, #25-058-CI) and suspended in DMEM/F12. The cell suspension was centrifuged at 300 × *g* for 5 min to form a cell pellet. The cells were then resuspended in 500 μL of PBS + 1% Penicillin-Streptomycin and passed through the filter of a sorting tube (Corning, #352235). Subsequently, 1 μL of DAPI was added. The tubes, now containing the labeled cells, were placed on ice and transported to the flow cytometry core. Sorting was performed based on DAPI negativity and GFP positivity/negativity, and the sorted cells were collected into complete culture medium. Following sorting, the cells were pelleted at 300 × *g* for 5 min and plated onto a 48-well plate coated with Geltrex (Thermo Fisher Scientific, #A1413302).

RNA/gDNA extraction for cDNA synthesis and CRISPR analysis

For RNA isolation, cultured NPCs and EVs from conditioned medium were processed using the miRNeasy Micro Kit (Qiagen, #217084, Germantown, MD, USA). For the isolation of exRNA from conditioned medium, as little as 500 μL from a confluent 48-well plate to 50 mL from multiple T75 flasks can be used. Conditioned medium should be on the cells for 48 h before isolation. Nanodrop (Thermo Fischer Scientific) was employed for RNA sample quantification, followed by reverse transcription using the Superscript IV VILO (Thermo Fisher Scientific, #11756050).

gDNA extraction from cultured hNPCs utilized the remaining sample post removal of the aqueous layer during RNA isolation. The protocol, adapted with modifications from the TRIzol reagent experimental protocol for DNA isolation (Invitrogen, 15596026, San Diego, CA, USA), involved the addition of 300 μL of 100% isopropanol to the sample. After a 30-min incubation at RT, the sample underwent centrifugation for 5 min at 2,000 × *g* at 4°C to pellet the DNA. The DNA pellet was resuspended in 1 mL of 0.1 M sodium citrate in 10% ethanol and incubated for 30 min and then spun at 2,000 × *g* for 5 min at 4°C. This step was repeated once. The pellet was then resuspended in 1 mL of 75% ethanol and incubated for 10–20 min. Following a 5-min centrifugation at 2,000 × *g* at 4°C, the pellet was air-dried and resuspended in 8 mM NaOH. pH adjustments were made as needed with HEPES.

Analysis of gene-editing outcomes from hNPCs

Isolated gDNA and cDNA were amplified for NGS analysis using the primers in Table 1. A portion of the PCR product was run on a gel to check for band size and appropriate amplification. PCR product was cleaned using the QIAquick PCR purification kit (Qiagen, #28106) and eluted in 35 μL of RNAase-free water. Samples were sent for next-generation sequencing (MGH CCIB DNA Core). After sequencing, the results were analyzed using CRISPResso2.

DYT1-TaqMan genotyping assay

A TaqMan SNP genotyping assay was custom designed by Thermo Fisher Scientific using the sequence GACATTGTAAGCAGAGT GGCTGAG[GAG/*]ATGACATTTTTCCCCAAAGAGGAG (assay ID: AN7D9YW). The VIC probe was specifically tailored to bind to the WT allele, while the FAM probe was designed to target the *TOR1A* DYT1 allele. The TaqMan Genotyping Master Mix (Applied Biosystems, #4371355) was then combined with the custom probes and DNA template before being run on the QuantStudio 3 machine. Subsequent analysis of the results was performed using the TaqMan Genotyper software.

EV isolation from culture medium and patient plasma

SEC

Conditioned cell culture medium was collected and centrifuged at 300 × *g* for 5 min to remove dead cells. The supernatant was filtered with syringe-driven 0.8-μm filter units (Millipore Sigma, #SLAAR33SS) and subsequently concentrated using Amicon Ultra 15-100k filters (EMD Millipore, #UFC910024, Billerica, MA). Subsequently, 500 μL of the concentrated medium was applied to IZON columns, specifically the qEVoriginal/70nm Legacy Column (IZON, #ICO-70, Medford, MA, USA), and fractions 1–30 were collected.

Fractions 6–11 and 15–20 were combined and utilized for the isolation of EVs and proteins, respectively.

exRNA isolation with ExoRNeasy kit

Isolated plasma from patients was provided. Five DYT1 patient, four symptom-presenting and one non-presenting, and three WT patient plasma samples were analyzed. exRNA was then isolated from both cell culture medium and plasma following the instructions provided with the exoRNeasy Serum/Plasma Starter Kit (Qiagen, #77023).

Preamplification of *TOR1A* for the DYT1 TaqMan genotyping assay from EVs

EVs exRNA isolated from plasma and cell culture medium underwent cDNA conversion and then were preamplified using the Phusion Hot Start Flex 2x Master Mix (New England Biolabs # MO536L) and the cDNA_preamplification primers indicated in Table 1. PCR cycles were used following manufacturer's instructions with the annealing temperature set to 64°C.

Cre-reporter cloning and lentiviral vector production

Cre-reporter construct was produced by doing a high-fidelity amplification of NanoLuc using Nluc primers listed in Table 1 from the NanoLuc outside and mCherry inside (ENoMi) construct.[15] The NanoLuc amplicon was cloned into a backbone regulated by an EF1-α promoter (Addgene plasmid #62732, Watertown, MA, USA) using Gibson assembly (New England Biolabs #M5510A) for 1 h at 50°C. Complete plasmid sequencing was carried out utilizing next-generation sequencing technology (MGH CCIB DNA Core) to check plasmid integrity.

Lentivirus vector production and transduction

Lentiviral vectors (LVVs) encoding Cre reporter were produced in HEK293T cells. 1×10^6 seeded cells were transfected with either of the constructs packaging plasmids and the transgene cassette was flanked by LVV long terminal repeats (LTRs). Twenty-four hours after transfection, cells were washed with 1× PBS (Boston BioProducts #BM-220, Ashland, MA, USA) and provided with a fresh medium. Seventy-two hours after transfection, the medium was collected and filtered with 0.45-μm filters (Thermo Fisher Scientific, #168-0045) followed by ultracentrifugation at 70,000 × *g*. The pellet was resuspended in 250 μL of 1% bovine serum albumin (BSA) (Sigma #A8412) in Opti-MEM and stored at −80°C.

Assembling gRNA3 and SaCas9-KKH into an AAV9 vector

Addgene plasmid #61591 was digested with enzyme BSA1 and ligated with annealed gRNA3 oligos. The ligation product was transformed into SURE cells (Agilent, #200227, Santa Clara, CA, USA). The correct vector was sent for packaging using PackGene (Houston, TX, USA).

Cell transduction

Stably transduced cell lines were generated by transducing hNPCs with Cre reporter lentivirus. Cells were incubated with lentivirus for 72 h, after which transfection medium was removed and fresh medium was added containing 1 μg/mL puromycin (Invitrogen, #ant-pr-1) to select for Cre-reporter transduced cells. After exposure to the appropriate selection antibiotics for a duration of 2 days, the cells that were stably transduced were cultured and expanded under standard conditions, with a limit of 20 passages.

Animal experiments

The Institutional Animal Care and Use Committee at Massachusetts General Hospital granted approval for all animal experimental procedures. NU/NU nude mice (Charles River Laboratories, Wilmington, MA, USA) were kept under a 12-h light/dark cycle with unrestricted access to food and water. Male mice, aged between 8 and 10 weeks, were randomly allocated to different experimental groups.

Stereotaxic injection into the mouse brain

Adult mice were anesthetized with 2.5% isoflurane[47] delivered in 100% oxygen via a nose cone. Stereotaxic injections into the left striatum were performed in relation to the bregma, with the following coordinates: anteroposterior, +0.52 mm; medial-lateral, +2.00 mm; dorsal-ventral, −2.5 mm. Mice were categorized into three groups throughout the project: AAV9-CRE, AAV9-SaCas9-KKH, and null empty AAV9. All groups of mice were concurrently implanted with Cre-reporter-transduced hNPCs. Specifically, 200,000 hNPCs were resuspended in 2 μL of AAV9-CRE (PackGene, C-8054 pAAV-CBA-Cre Clone 686.2), anti-DYT1 AAV9-SaCas9-KKH, or AAV9-null and were implanted at an infusion rate of 0.25 μL/min using a 10-μL 26s-gauge Hamilton syringe (Reno, NV, USA). After the infusion was completed, the needle was allowed to remain in place for an additional 3 min prior to complete removal from mouse brains, ensuring proper procedure completion.

Mouse brain tissue preparation for immunohistochemistry, DNA extraction, and NGS

Twenty-one days post injection, mice were euthanized under deep anesthesia induced by a combination of xylazine and ketamine (10 mg/kg and 100 mg/kg, respectively) following the protocol previously outlined.[48] For immunohistochemistry, mice underwent cardiac perfusion with 1× PBS, followed by 4% paraformaldehyde, and brains were harvested and cryopreserved at −80°C using optimal cutting temperature (OCT) compound (Neg-50 #6502, Expredia, Kalamazoo, MI, USA) for subsequent coronal sectioning onto glass slides. Coronal sections of mouse brains, each 16 μm thick, were obtained using a freezing cryostat (Leica Microsystems, CM3050S, Deer Park, IL, USA) and mounted on slides.

In the case of bioluminescence assays and gDNA extraction, mouse brains were promptly collected and flash-frozen with dry ice to preserve RNA integrity. Brain tissue around the injection site was coronally sectioned with a thickness of 100 μm using a freezing cryostat and collected in individual tubes as per the method described by Maalouf et al. Each 100-μm brain section was subsequently homogenized in 200 μL of Nano-Glo luciferase assay buffer (Promega, Madison, WI, USA). Thirty microliters of this homogenate was employed for bioluminescence measurement, while the remaining sample was

utilized for gDNA extraction using the DNeasy Blood and Tissue Kit (Qiagen, #69504) and subsequent expression analysis. gDNA isolated from the mouse brain was amplified in a two-step process, first using primers binding to the human and mouse TOR1A alleles (gDNA_preamp, Table 1). This was followed by amplification with human-specific primers that did not bind to the mouse allele to ensure analysis of only our implanted cells (CRISP_amp, Table 1). This two-step process was crucial to ensure the detection of the implanted cells.

exRNA isolation from mouse plasma and NGS preparation

Mouse blood was obtained from the heart and centrifuged at 1,500 × *g* for 10 min. The resulting supernatant was centrifuged at 2,500 × *g* for 15 min to collect plasma. This plasma was subsequently filtered using 0.8-μm filters. ExRNA was then isolated following the instructions provided with the exoRNeasy Serum/Plasma Starter Kit (Qiagen, #77023).

Immunohistochemistry

Brain sections underwent post-fixation with 4% paraformaldehyde for 20 min, followed by three washes with 1× PBS and a 30-min incubation in blocking solution (PBS with 0.1% Triton X-100, USB #22686, Cleveland, OH, USA) containing 10% normal goat serum (Sigma). Subsequently, the sections were incubated overnight at 4°C in blocking solution with primary antibodies: rabbit anti-RFP (Abcam, ab124754, 1:400, Cambridge, MA, USA) and fluorescein isothiocyanate (FITC) anti-GFP (Abcam, ab6662, 1:200). After PBS washing, the sections were incubated for 1 h at RT with the appropriate secondary antibodies: goat anti-rabbit IgG (Invitrogen, A-21428, 1:1,000) diluted in blocking solution, or with secondary antibody alone. Following another wash with 1× PBS, the sections were mounted on glass slides using ProLong Diamond Antifade Mountant (Invitrogen, P36965). Immunofluorescence was observed and captured using a Yokogawa CSU-W1 spinning disk coupled to a Nikon Eclipse Ti2 confocal microscope.

Quantification of RFP/GFP signal in hNPC Cre-reporter implanted cells

Primary segmentation of cells was done via Cellpose cell detector using the built-in cytoplasm model (estimated cell diameter 10–20 μm)[49] implemented in TrackMate plugin, a Fiji plugin.[50,51] Next, false positives and false negatives were corrected manually. In cases where Cellpose segmentation failed, positive cells were manually segmented. The total number of eGFP-positive cells and DsRed-positive cells were measured. An automated approach was employed to quantify eGFP/dsRed expression in CRE-reporter implanted hNPCs injected with AAV9-CBA-CRE ($n = 4$) or AAV9-null ($n = 3$). Two to three images from each brain were capturing using a 20×/0.75 objective (Plan Apo λ, Nikon). [protein1] was excited using a 488-nm laser light and detected with a 535 ± 40-nm emission filter while [protein2] was excited with 561-nm laser light and detected with a 603 ± 53 emission filter, and subsequent maximal projections were generated for analysis. Fields of view covering the implanted hNPCs were analyzed in coronal sections at 20× magnification. Leveraging deep-learning techniques, Cellpose algorithm effectively performed robust cell segmentation, accurately identifying and delineating individual cells or cell-like structures based on their distinct features.[39] This powerful capability was integrated with TrackMate, a Fiji plugin for precise cell tracking and analysis. Cells with mean whole-cell signal 2 SD above background were considered for further analysis. Some images were quantified manually instead of with Cellpose since the cells exhibited varying morphologies as a result of differentiation. The total number of eGFP-positive and DsRed-positive CRE-reporter implanted hNPCs was calculated followed by their percentages in each image. The mean values of all eGFP-positive hNPCs per group was compared to the mean value of DsRed-positive hNPCs using a two-way ANOVA and Sidak's multiple comparisons test.

DATA AVAILABILITY

The authors confirm that the data supporting the findings are available within the article and its supplementary material. Raw data that support the findings reported in this study are available upon reasonable request. The data discussed in this publication have been deposited in NCBI's Gene Expression Omnibus and are accessible through GEO series accession number GSE288087.

ACKNOWLEDGMENTS

We especially thank Xandra O. Breakefield from MGH for her invaluable insights into DYT1 dystonia. Her pioneering research in gene therapy and EVs has significantly advanced our understanding and treatment of this condition. Her expertise has been instrumental in driving the field of neurogenetics forward. We thank all members of the Breyne laboratory for their suggested ideas during laboratory meetings. We thank Ms. Suzanne McDavitt for her skilled editorial assistance. We thank Dr. Lilian Cruz for her input into the concepts and tools used in these studies. K.B. is funded by NIH K22 CA2802019-01 and DOD HT9425-24-1-0119, B.P.K. was supported by the Kayden-Lambert MGH Research Scholar Award and NIH DP2-CA281401, and D.R.R. was supported by Friedreich's Ataxia Research Alliance (FARA) and fara Australia.

AUTHOR CONTRIBUTIONS

K.E.M., D.M.F., and K.B. performed experiments, analyzed data, and wrote the paper. E.A.H., R.J.S., and M.S.M. aided and performed confocal experiments and analyzed data. N.S. provided plasma samples from patients and controls. T.X. generated lentivirus vectors for this project. D.R.-R. and B.P.K. advised on genome editing, generated the gRNAs used, and helped edit the manuscript. C.A.V. and D.C.B. provided hNPCs and offered valuable insight into hNPCs maintenance and the DYT1 disease. K.B. conceptualized the study, planned and supervised experiments, and wrote and edited the paper.

DECLARATION OF INTERESTS

An invention disclosure (2024-409) has been filed for findings described in this manuscript. B.P.K. is an inventor on patents or patent applications filed by MGB that describe genome engineering technologies. B.P.K. is a consultant for EcoR1 capital and Novartis Venture Fund and is on the scientific advisory boards of Acrigen Biosciences, Life Edit Therapeutics, and Prime Medicine. B.P.K. has a financial interest in Prime Medicine, Inc., a company developing therapeutic CRISPR-Cas technologies for gene editing. B.P.K.'s interests were reviewed and managed by MGH and MGB in accordance with their conflict-of-interest policies.

SUPPLEMENTAL INFORMATION

Supplemental information can be found online at https://doi.org/10.1016/j.omtn.2025.102466.

REFERENCES

1. Breakefield, X.O., Blood, A.J., Li, Y., Hallett, M., Hanson, P.I., and Standaert, D.G. (2008). The pathophysiological basis of dystonias. Nat. Rev. Neurosci. *9*, 222–234. https://doi.org/10.1038/nrn2337.

2. Tsuboi, T., Jabarkheel, Z., Foote, K.D., Okun, M.S., and Wagle Shukla, A. (2019). Importance of the initial response to GPi deep brain stimulation in dystonia: A nine year quality of life study. Parkinsonism Relat. Disorders *64*, 249–255. https://doi.org/10.1016/j.parkreldis.2019.04.024.

3. Tsuboi, T., Cif, L., Coubes, P., Ostrem, J.L., Romero, D.A., Miyagi, Y., Lozano, A.M., De Vloo, P., Haq, I., Meng, F., et al. (2020). Secondary Worsening Following DYT1 Dystonia Deep Brain Stimulation: A Multi-country Cohort. Front. Hum. Neurosci. *14*, 242. https://doi.org/10.3389/fnhum.2020.00242.

4. Caffall, Z.F., Wilkes, B.J., Hernández-Martinez, R., Rittiner, J.E., Fox, J.T., Wan, K.K., Shipman, M.K., Titus, S.A., Zhang, Y.-Q., Patnaik, S., et al. (2021). The HIV protease inhibitor, ritonavir, corrects diverse brain phenotypes across development in mouse model of DYT-TOR1A dystonia. Sci. Transl. Med. *13*, eabd3904. https://doi.org/10.1126/scitranslmed.abd3904.

5. Jung, I.-H., Chang, K.W., Park, S.H., Chang, W.S., Jung, H.H., and Chang, J.W. (2022). Complications After Deep Brain Stimulation: A 21-Year Experience in 426 Patients. Front. Aging Neurosci. *14*, 819730. https://doi.org/10.3389/fnagi.2022.819730.

6. Nance, E., Pun, S.H., Saigal, R., and Sellers, D.L. (2022). Drug delivery to the central nervous system. Nat. Rev. Mater. *7*, 314–331. https://doi.org/10.1038/s41578-021-00394-w.

7. Leung, J.C., Klein, C., Friedman, J., Vieregge, P., Jacobs, H., Doheny, D., Kamm, C., DeLeon, D., Pramstaller, P.P., Penney, J.B., et al. (2001). Novel mutation in the TOR1A (DYT1) gene in atypical early onset dystonia and polymorphisms in dystonia and early onset parkinsonism. Neurogenetics *3*, 133–143. https://doi.org/10.1007/s100480100111.

8. Doheny, D., Danisi, F., Smith, C., Morrison, C., Velickovic, M., De Leon, D., Bressman, S.B., Leung, J., Ozelius, L., Klein, C., et al. (2002). Clinical findings of a myoclonus-dystonia family with two distinct mutations. Neurology *59*, 1244–1246. https://doi.org/10.1212/wnl.59.8.1244.

9. Calakos, N., Patel, V.D., Gottron, M., Wang, G., Tran-Viet, K.-N., Brewington, D., Beyer, J.L., Steffens, D.C., Krishnan, R.R., and Züchner, S. (2010). Functional evidence implicating a novel TOR1A mutation in idiopathic, late-onset focal dystonia. J. Med. Genet. *47*, 646–650. https://doi.org/10.1136/jmg.2009.072082.

10. Fan, Y., Si, Z., Wang, L., and Zhang, L. (2023). DYT-TOR1A dystonia: an update on pathogenesis and treatment. Front. Neurosci. *17*, 1216929. https://doi.org/10.3389/fnins.2023.1216929.

11. Ozelius, L.J., Hewett, J.W., Page, C.E., Bressman, S.B., Kramer, P.L., Shalish, C., de Leon, D., Brin, M.F., Raymond, D., Corey, D.P., et al. (1997). The early-onset torsion dystonia gene (DYT1) encodes an ATP-binding protein. Nat. Genet. *17*, 40–48. https://doi.org/10.1038/ng0997-40.

12. Cruz, L., György, B., Cheah, P.S., Kleinstiver, B.P., Eimer, W.A., Garcia, S.P., Sharma, N., Ozelius, L.J., Bragg, D.C., Joung, J.K., et al. (2020). Mutant Allele-Specific CRISPR Disruption in DYT1 Dystonia Fibroblasts Restores Cell Function. Mol. Ther. Nucleic Acids *21*, 1–12. https://doi.org/10.1016/j.omtn.2020.05.009.

13. Kleinstiver, B.P., Prew, M.S., Tsai, S.Q., Nguyen, N.T., Topkar, V.V., Zheng, Z., and Joung, J.K. (2015). Broadening the targeting range of Staphylococcus aureus CRISPR-Cas9 by modifying PAM recognition. Nat. Biotechnol. *33*, 1293–1298. https://doi.org/10.1038/nbt.3404.

14. Rufino-Ramos, D., Lule, S., Mahjoum, S., Ughetto, S., Cristopher Bragg, D., Pereira de Almeida, L., Breakefield, X.O., and Breyne, K. (2022). Using genetically modified extracellular vesicles as a non-invasive strategy to evaluate brain-specific cargo. Biomaterials *281*, 121366. https://doi.org/10.1016/j.biomaterials.2022.121366.

15. Maalouf, K.E., Vaine, C.A., Frederick, D.M., Yoshinaga, A., Obuchi, W., Mahjoum, S., Nieland, L., Al Ali, J., Bragg, D.C., Breakefield, X.O., and Breyne, K. (2023). Tracking human neurologic disease status in mouse brain/plasma using reporter-tagged, EV-associated biomarkers. Mol. Ther. *31*, 2206–2219. https://doi.org/10.1016/j.ymthe.2023.05.011.

16. Nogueras-Ortiz, C.J., Eren, E., Yao, P., Calzada, E., Dunn, C., Volpert, O., Delgado-Peraza, F., Mustapic, M., Lyashkov, A., Rubio, F.J., et al. (2024). Single-extracellular vesicle (EV) analyses validate the use of L1 Cell Adhesion Molecule (L1CAM) as a reliable biomarker of neuron-derived EVs. J. Extracell. Vesicles *13*, e12459. https://doi.org/10.1002/jev2.12459.

17. Chatterjee, M., Özdemir, S., Fritz, C., Möbius, W., Kleineidam, L., Mandelkow, E., Biernat, J., Doğdu, C., Peters, O., Cosma, N.C., et al. (2024). Plasma extracellular vesicle tau and TDP-43 as diagnostic biomarkers in FTD and ALS. Nat. Med. *30*, 1771–1783. https://doi.org/10.1038/s41591-024-02937-4.

18. Clement, K., Rees, H., Canver, M.C., Gehrke, J.M., Farouni, R., Hsu, J.Y., Cole, M.A., Liu, D.R., Joung, J.K., Bauer, D.E., and Pinello, L. (2019). CRISPResso2 provides accurate and rapid genome editing sequence analysis. Nat. Biotechnol. *37*, 224–226. https://doi.org/10.1038/s41587-019-0032-3.

19. O'Brien, K., Breyne, K., Ughetto, S., Laurent, L.C., and Breakefield, X.O. (2020). RNA delivery by extracellular vesicles in mammalian cells and its applications. Nat. Rev. Mol. Cell Biol. *21*, 585–606. https://doi.org/10.1038/s41580-020-0251-y.

20. Sadik, N., Cruz, L., Gurtner, A., Rodosthenous, R.S., Dusoswa, S.A., Ziegler, O., Van Solinge, T.S., Wei, Z., Salvador-Garicano, A.M., Gyorgy, B., et al. (2018). Extracellular RNAs: A New Awareness of Old Perspectives. Methods Mol. Biol. *1740*, 1–15. https://doi.org/10.1007/978-1-4939-7652-2_1.

21. Gruner, H.N., and McManus, M.T. (2021). Examining the evidence for extracellular RNA function in mammals. Nat. Rev. Genet. *22*, 448–458. https://doi.org/10.1038/s41576-021-00346-8.

22. Böing, A.N., van der Pol, E., Grootemaat, A.E., Coumans, F.A.W., Sturk, A., and Nieuwland, R. (2014). Single-step isolation of extracellular vesicles by size-exclusion chromatography. J. Extracell. Vesicles *3*, 23430. https://doi.org/10.3402/jev.v3.23430.

23. Yang, Z.X., Fu, Y.W., Zhao, J.J., Zhang, F., Li, S.A., Zhao, M., Wen, W., Zhang, L., Cheng, T., Zhang, J.P., and Zhang, X.B. (2023). Superior Fidelity and Distinct Editing Outcomes of SaCas9 Compared with SpCas9 in Genome Editing. Dev. Reprod. Biol. *21*, 1206–1220. https://doi.org/10.1016/J.GPB.2022.12.003.

24. Chakrabarty, P., Rosario, A., Cruz, P., Siemienski, Z., Ceballos-Diaz, C., Crosby, K., Jansen, K., Borchelt, D.R., Kim, J.-Y., Jankowsky, J.L., et al. (2013). Capsid Serotype and Timing of Injection Determines AAV Transduction in the Neonatal Mice Brain. PLoS One *8*, e67680. https://doi.org/10.1371/journal.pone.0067680.

25. Hudry, E., and Vandenberghe, L.H. (2019). Therapeutic AAV Gene Transfer to the Nervous System: A Clinical Reality. Neuron *101*, 839–862. https://doi.org/10.1016/j.neuron.2019.02.017.

26. Nieland, L., Vrijmoet, A.B., Jetten, I.W., Rufino-Ramos, D., de Reus, A.J.E.M., Breyne, K., Kleinstiver, B.P., Maguire, C.A., Broekman, M.L.D., Breakefield, X.O., and Abels, E.R. (2025). CRISPR targeting of mmu-miR-21a through a single adeno-associated virus vector prolongs survival of glioblastoma-bearing mice. Mol. Ther. *33*, 133–151. https://doi.org/10.1016/J.YMTHE.2024.11.023.

27. Im, W., Moon, J., and Kim, M. (2016). Applications of CRISPR/Cas9 for Gene Editing in Hereditary Movement Disorders. J. Mov. Disord. *9*, 136–143. https://doi.org/10.14802/jmd.16029.

28. A Clinical Trial of PR001 (LY3884961) in Patients With Peripheral Manifestations of Gaucher Disease (PROCEED) | Clinical Research Trial Listing. https://www.centerwatch.com/clinical-trials/listings/NCT05487599/a-clinical-trial-of-pr001-ly3884961-in-patients-with-peripheral-manifestations-of-gaucher-disease-proceed.

29. Campos, L.J., Arokiaraj, C.M., Chuapoco, M.R., Chen, X., Goeden, N., Gradinaru, V., and Fox, A.S. (2023). Advances in AAV technology for delivering genetically encoded cargo to the nonhuman primate nervous system. Curr. Res. Neurobiol. *4*, 100086. https://doi.org/10.1016/J.CRNEUR.2023.100086.

30. Goertsen, D., Flytzanis, N.C., Goeden, N., Chuapoco, M.R., Cummins, A., Chen, Y., Fan, Y., Zhang, Q., Sharma, J., Duan, Y., et al. (2021). AAV capsid variants with brain-wide transgene expression and decreased liver targeting after intravenous delivery in mouse and marmoset. Nat. Neurosci. *25*, 106–115. https://doi.org/10.1038/s41593-021-00969-4.

31. Asokan, A., and Shen, S. (2023). Redirecting AAV vectors to extrahepatic tissues. Mol. Ther. *31*, 3371–3375. https://doi.org/10.1016/j.ymthe.2023.10.005.

32. Wang, C., Pan, C., Yong, H., Wang, F., Bo, T., Zhao, Y., Ma, B., He, W., and Li, M. (2023). Emerging non-viral vectors for gene delivery. J. Nanobiotechnol. *21*, 272. https://doi.org/10.1186/S12951-023-02044-5.

33. Pacesa, M., Pelea, O., and Jinek, M. (2024). Past, present, and future of CRISPR genome editing technologies. Cell *187*, 1076–1100. https://doi.org/10.1016/J.CELL.2024.01.042.

34. Albanese, A., Bhatia, K., Bressman, S.B., Delong, M.R., Fahn, S., Fung, V.S.C., Hallett, M., Jankovic, J., Jinnah, H.A., Klein, C., et al. (2013). Phenomenology and

classification of dystonia: a consensus update. Mov. Disord. *28*, 863–873. https://doi.org/10.1002/mds.25475.

35. Laurie Ozelius, P., and Naomi Lubarr, M. (2016). DYT1 Early-Onset Isolated Dystonia (GeneReviews® [Internet]).
36. King, C.S., Caffall, Z.F., Soderblom, E.J., and Calakos, N. (2023). DYT-TOR1A genotype alters extracellular vesicle composition in murine cell model and shows potential for biomarker discovery. Dystonia *2*, 11053. https://doi.org/10.3389/dyst.2023.11053.
37. Thompson, A.G., Gray, E., Heman-Ackah, S.M., Mäger, I., Talbot, K., Andaloussi, S.E., Wood, M.J., and Turner, M.R. (2016). Extracellular vesicles in neurodegenerative disease - pathogenesis to biomarkers. Nat. Rev. Neurol. *12*, 346–357. https://doi.org/10.1038/nrneurol.2016.68.
38. Abels, E.R., and Breakefield, X.O. (2016). Introduction to Extracellular Vesicles: Biogenesis, RNA Cargo Selection, Content, Release, and Uptake. Cell. Mol. Neurobiol. *36*, 301–312. https://doi.org/10.1007/s10571-016-0366-z.
39. Kostyushev, D., Kostyusheva, A., Brezgin, S., Smirnov, V., Volchkova, E., Lukashev, A., and Chulanov, V. (2020). Gene Editing by Extracellular Vesicles. Int. J. Mol. Sci. *21*, 7362. https://doi.org/10.3390/ijms21197362.
40. Yao, X., Lyu, P., Yoo, K., Yadav, M.K., Singh, R., Atala, A., and Lu, B. (2021). Engineered extracellular vesicles as versatile ribonucleoprotein delivery vehicles for efficient and safe CRISPR genome editing. J. Extracell. Vesicles *10*, e12076. https://doi.org/10.1002/jev2.12076.
41. Chen, R., Huang, H., Liu, H., Xi, J., Ning, J., Zeng, W., Shen, C., Zhang, T., Yu, G., Xu, Q., et al. (2019). Friend or Foe? Evidence Indicates Endogenous Exosomes Can Deliver Functional gRNA and Cas9 Protein. Small *15*, e1902686. https://doi.org/10.1002/smll.201902686.
42. Leandro, K., Rufino-Ramos, D., Breyne, K., di Ianni, E., Lopes, S.M., Jorge Nobre, R., Kleinstiver, B.P., Perdigão, P.R.L., Breakefield, X.O., and Pereira de Almeida, L. (2024). Exploring the potential of cell-derived vesicles for transient delivery of gene editing payloads. Adv. Drug Deliv. Rev. *211*, 115346. https://doi.org/10.1016/j.addr.2024.115346.
43. Rufino-Ramos, D., Leandro, K., Perdigão, P.R.L., O'Brien, K., Pinto, M.M., Santana, M.M., van Solinge, T.S., Mahjoum, S., Breakefield, X.O., Breyne, K., and Pereira de Almeida, L. (2023). Extracellular communication between brain cells through functional transfer of Cre mRNA. Preprint at bioRxiv. https://doi.org/10.1101/2023.01.29.525937.
44. Rufino-Ramos, D., Lule, S., Mahjoum, S., Ughetto, S., Cristopher Bragg, D., Pereira de Almeida, L., Breakefield, X.O., and Breyne, K. (2022). Using genetically modified extracellular vesicles as a non-invasive strategy to evaluate brain-specific cargo. Biomaterials *281*, 121366. https://doi.org/10.1016/j.biomaterials.2022.121366.
45. Ito, N., Hendriks, W.T., Dhakal, J., Vaine, C.A., Liu, C., Shin, D., Shin, K., Wakabayashi-Ito, N., Dy, M., Multhaupt-Buell, T., et al. (2016). Decreased N-TAF1 expression in X-linked dystonia-parkinsonism patient-specific neural stem cells. Dis. Model. Mech. *9*, 451–462. https://doi.org/10.1242/dmm.022590.
46. Al Ali, J., Vaine, C.A., Shah, S., Campion, L., Hakoum, A., Supnet, M.L., Acuña, P., Aldykiewicz, G., Multhaupt-Buell, T., Ganza, N.G.M., et al. (2021). <scp> TAF1 </scp> Transcripts and Neurofilament Light Chain as Biomarkers for X-linked Dystonia-Parkinsonism. Mov. Disord. *36*, 206–215. https://doi.org/10.1002/mds.28305.
47. Henry, R.T., and Casto, R. (1989). Simple and inexpensive delivery of halogenated inhalation anesthetics to rodents. Am. J. Physiol. *257*, R668–R671. https://doi.org/10.1152/ajpregu.1989.257.3.R668.
48. Xu, Q., Ming, Z., Dart, A.M., and Du, X.J. (2007). Optimizing dosage of ketamine and xylazine in murine echocardiography. Clin. Exp. Pharmacol. Physiol. *34*, 499–507. https://doi.org/10.1111/j.1440-1681.2007.04601.x.
49. Stringer, C., Wang, T., Michaelos, M., and Pachitariu, M. (2021). Cellpose: a generalist algorithm for cellular segmentation. Nat. Methods *18*, 100–106. https://doi.org/10.1038/s41592-020-01018-x.
50. Schindelin, J., Arganda-Carreras, I., Frise, E., Kaynig, V., Longair, M., Pietzsch, T., Preibisch, S., Rueden, C., Saalfeld, S., Schmid, B., et al. (2012). Fiji: an open-source platform for biological-image analysis. Nat. Methods *9*, 676–682. https://doi.org/10.1038/nmeth.2019.
51. Tinevez, J.-Y., Perry, N., Schindelin, J., Hoopes, G.M., Reynolds, G.D., Laplantine, E., Bednarek, S.Y., Shorte, S.L., and Eliceiri, K.W. (2017). TrackMate: An open and extensible platform for single-particle tracking. Methods *115*, 80–90. https://doi.org/10.1016/j.ymeth.2016.09.016.